Effect of surface functionalization and physical properties of the nano-inclusions on thermal conductivity enhancement in organic phase change material

Amit Kumar Mishra[1], Barid Baran Lahiri[1] and John Philip[1*]

[1]Smart Materials Section, Corrosion Science and Technology Division, Materials Characterization Group, Metallurgy and Materials Group, Indira Gandhi Centre for Atomic Research, HBNI, Kalpakkam, Tamil Nadu, India, PIN 603102

[*]Corresponding author
Dr. John Philip
Head, Smart Materials Section
Head, Corrosion Science and Technology Division
Email: philip@igcar.gov.in
Phone: 044-27480500 Ext. 26447

Supporting Information

Section S1

Calculations of ϕ_{bb}, ϕ_{de} and ϕ_c

Let, d_f be the fractal dimension of a cluster of nano-inclusions. Then the number of nano-inclusions within a cluster is expressed as $N_c = (R_g / a)^{d_f}$. Let ϕ_p be the total volume fraction of nano-inclusions added to the PCM. Then $\phi_p = \phi_c \times \phi_a$, where $\phi_{c \text{ and}}\ \phi_a$ indicate the volume fraction of nano-inclusion within a cluster and volume fraction of cluster, respectively. From fractal analyses, it can be shown that $\phi_c = (R_g / a)^{d_f - 3}$ and volume fraction of nano-inclusions within a cluster that belong to the back bone (ϕ_{bb}) is given by $\phi_{bb} = (R_g / a)^{d_1 - 3}$, where d_1 is the chemical dimension (ranging from 1 to d_f) [25]. Then the volume faction of nano-inclusion, within a cluster, belonging to dead-ends (ϕ_{de}) is given by $\phi_{de} = \phi_c - \phi_{bb}$ [25].

Section S2

Characterization results for the nano-inclusions

Figures S1a-e show the transmission electron microscopy (TEM) images of CBNP, NiNP, CuNP, AgNW and MWCNT, respectively. **Fig. S1f** shows the scanning electron microscopy (SEM) image of GNP. The scale bars are shown along with the electron microscopy images, which were obtained from the respective suppliers. The outer diameter and length of AgNW were ~ 100 nm and < 500 nm, respectively, whereas the lateral dimension of GNP was ~ 2 μm. On the other hand, the outer diameter and length of MWCNT were < 8 nm and ~ 20-30 μm, respectively. **Fig. S2a** shows the powder XRD pattern of NiNP at room temperature, where clear Bragg reflection peaks corresponding to (111), (200) and (220) planes of FCC nickel were observed for 2θ values of 44.5, 51.8 and 76.4 ^{0}, respectively (JCPDS 04-0850) [31]. The average crystallite size, determined from the strongest reflection peak of (111) plane

using Scherrer's equation, was found to be ~ 29 (±3) nm. **Fig. S2b** shows the powder XRD pattern of CuNP at room temperature, where the Bragg reflection peaks indicated the presence of elemental Cu and monovalent and divalent oxides of Cu (Cu_2O and CuO). The Bragg reflection peaks corresponding to (111), (200) and (220) planes of FCC Cu were observed at 2θ values of 43.4, 50.5 and 74.1 0, respectively (JCPDS 71-4610) [32]. The average crystallite size obtained from the strongest reflection peak of (111) plane, using Scherrer's equation, was found to be ~ 13 (± 2) nm. **Figs. S2c-d** show the size distributions for the NiNP and CuNP samples obtained from TEM image analyses (**Figs. S1b-c**, respectively). The average sizes were obtained as 23.4 ± 2.3 and 12.8 ± 2.8 nm for NiNP and CuNP, respectively, which were found to be in good agreement with the average crystallite sizes, obtained from the XRD patterns. The scattering intensity (I(q)), obtained from small angle X-ray scattering experiments were analyzed using a spherical model: $I(q) = (\Delta\rho)^2 V^2 [3\frac{\sin(\frac{qd_{NP}}{2}) - (\frac{qd_{NP}}{2})\cos(\frac{qd_{NP}}{2})}{(\frac{qd_{NP}}{2})^3}]$, where q, Δρ, V and d_{NP} indicate scattering wave vector, electron density difference between the nanoparticles and the surrounding medium, nanoparticle volume and diameter of the nanoparticle, respectively [33]. The distance distribution function (P(r)), was quantified from the Fourier transform of the scattering intensity [$P(r) = \frac{2}{\pi}\int_0^\infty I(q)qrSin(qr)e^{-Bq^2}dq$, where B is a numerical factor related to the termination effect of Fourier transform]. **Fig. S2e** shows the variation of P(r) as a function of size for CBNP and GNP. The most probable sizes were found to be 21 (± 2) and 12.3 (± 2) nm for CBNP and GNP, respectively. The **inset of Fig. S2e** shows the variation of ln[I(q)] as a function of ln(q) in the case of GNP and it was observed that in the high q region (Porod's region), ln[I(q)] varied linearly with ln(q) with a slope of -2.63 ± 0.01. For perfectly spherical nanoparticles, I(q) ~ q^{-4} and the slope of ln[I(q)] vs. ln(q) is expected to be -4,

whereas a slope of -2.63 indicated the presence of fractal dimensions in the case of GNP [33], which was in agreement with the results reported elsewhere [6, 34]. **Fig. S2f** shows the hydrodynamic size distributions of NiNP, CuNP and CBNP, dispersed in hexadecane at room temperature, where unimodal size distributions were obtained. The average hydrodynamic sizes were 295 ± 59, 296 ± 82 and 615 ± 141 nm for NiNP, CuNP and CBNP, respectively, which were significantly higher than the nanoparticle sizes obtained from XRD, TEM and SAXS. This indicated significant aggregation of the nano-inclusions on dispersion in hexadecane. This was also evident from the increase of average hydrodynamic sizes as a function of time, which is shown in the **inset of Fig. S2f**. It can be also seen from **Fig. S2f** that the average aggregate size was significantly higher for CBNP, which was attributed to the formation of aciniform aggregates of the primary particles (nodules), as reported earlier [35].

Figure S3 shows the FTIR spectra of the oleic acid capped CBNP, NiNP, AgNW, and GNP nano-inclusions, dispersed in hexadecane. For comparison, the FTIR spectra of pure oleic acid and hexadecane are also shown in **Fig. S3**. The major absorption bands were indexed and **Table S1** shows the details.

It can be seen from **Fig. S3** and **Table S1** that the strong absorption band, at1716 cm^{-1}, for the pure oleic acid (corresponding to the stretching of carbonyl group) was missing for the oleic acid capped nano-inclusions, where two new absorption bands appeared at 1667 and 1598 cm^{-1} (corresponding to the asymmetric and symmetric stretching of $–COO^-$, respectively) [37]. The difference between the symmetric and asymmetric bands was ~ 69 cm^{-1}, indicating the formation of chelating bidentate on the surface of the nano-inclusions, upon coating with oleic acid due to strong electronic interaction of the polar carboxylic head group of oleic acid with the nano-inclusions [37]. It can be further seen from **Fig. S3** that the major absorption

bands were not shifted for the PCM loaded with various nano-inclusions, which clearly indicated the absence of any chemical reaction between the PCM and the nano-inclusions.

Section S3

Model for thermal conductivity enhancement of GNP nano-inclusions and effect of oleic acid coating

Effective thermal conductivity enhancements in the PCM loaded with GNP and GNP-UC were analyzed using the model proposed by Chu et al. [53]. This model considers an isotropic composite structure with GNP inclusions distributed randomly and the interfacial thermal losses are represented by an average interfacial thermal resistance (R_K) between the GNP and the composite. Hence, the GNP is assumed as a two-dimensional plate of intrinsic thermal conductivity (k_g), surrounded by a hypothetical layer of material with thermal resistance of R_K. Hence, the effective thermal conductivity of GNP can be expressed by the following equations [53].

$$k_x = \frac{k_g}{(2R_K k_g)/L + 1} \tag{S1}$$

$$k_z = \frac{k_g}{(2R_K k_g)/L_t + 1} \tag{S2}$$

Here, k_x and k_z indicate effective thermal conductivity along the in-plane and through thickness directions, respectively. L and L_t indicate length and thickness of the GNP, respectively. For $k_x >> k_z$, using micromechanics theory, it can be shown that the effective thermal conductivity (k) of a composite loaded with randomly distributed GNP inclusions can be obtained from the following equation [53].

$$\frac{k}{k_m} = \frac{\phi}{3}\left[\frac{2}{H + \frac{1}{(k_x/k_m)-1}} + \frac{1}{\frac{1-H}{2} + \frac{1}{(k_z/k_m)-1}}\right] + 1 \tag{S3}$$

Here, k_m is the thermal conductivity of the composite matrix (without any nano-inclusions) in the solid state, ϕ is the effective volume fraction of the nano-inclusions (after cluster homogenization) and H is a geometrical factor that depends on the aspect ratio ($p = L/L_t$) and can be expressed by the following equation [53].

$$H = \frac{\ln(p+\sqrt{p^2-1})p}{\sqrt{(p^2-1)^3}} - \frac{1}{p^2-1} \quad \text{(S4)}$$

For large values of thermal anisotropy and aspect ratio, Eq. S3 can be reduced to a simplified form, which is expressed by the following expression [53].

$$\frac{k}{k_m} = \frac{2\phi/3}{H + \frac{1}{(k_x/k_m)-1}} + 1 \quad \text{(S5)}$$

Theoretical values of k/k_m, in the case of PCM loaded with GNP and GNP-UC, were computed using Eq. S5, where the value of R_K was considered as 5×10^{-8} m^2KW^{-1} for GNP-UC [54].

Section S4

Kaptiza resistance for coated nano-inclusions

Due to the presence of oleic acid capping on the surface, the Kapitza resistance of the surface functionalized GNP nano-inclusions were expected to be higher and the value was approximated based on the following equation for thermal conductivity of coated nano-spheres [49].

$$\frac{k_{sp}}{k_s} = 1 + \frac{3\phi_s(k_p - k_s)}{3k_s + (1-\phi_s)(k_p - k_m)} \quad \text{(S6)}$$

Here, k_{sp}, k_p and k_s indicate thermal conductivity of the surface modified nanoparticles, uncoated nanoparticles and that of surfactant (i.e. coating material), respectively. ϕ_s is expressed as $\phi_s = [a_p/(a_p+\delta_s)]^3$, where a_p and δ_s indicate radius of the nanoparticle and coating thickness, respectively [49]. The typical thickness of oleic acid coating was considered as 2 nm

[8]. The values of k_{sp}/k_s and k_p/k_s were obtained as 51.46 and 62.29, respectively, which clearly showed that the effective thermal conductivity of the coated nanoparticles was lower, as compared to the uncoated nanoparticles. Moreover, for the above calculations, a spherical morphology of the nano-inclusions was assumed, whereas, GNP agglomerates are fractal in nature with larger surface to volume ratio [6, 34]. The enhancement in surface area to volume ratio from a sphere to a cube is ~ 1.24 (surface area to volume ratios of a sphere and cube are ~ 4.836 and 6, respectively). Hence, the Kaptiza resistance for the oleic acid functionalized GNP was approximated as $5 \times 10^{-8} \times 1.21$ (effect of surface functionalization with spherical morphology approximation) $\times$ 1.24 (correction factor for non-spherical morphology) ~ 8×10^{-8} m^2KW^{-1}. This value was then plugged in Eq. S5 to obtain the theoretical values of k/k_m.

Section S5

Description of the characterization techniques

Room temperature powder X-ray diffraction (XRD) studies were carried out on NiNP and CuNP samples in the 2θ range of $20\text{-}80^0$ using a Rigaku X-ray diffractometer, operating in the Bragg-Brentano geometry using Cu-Kα radiation (wavelength = 1.5416 Å). The scan rate and step size were fixed at 2^0 per minute and 0.02^0, respectively. The average crystallite size (d_{cryst}) was measured from the most intense XRD peak using Scherrer's formula: $d_{cryst} = 0.9\lambda/\beta\cos\theta$, where λ, θ and β indicate X-ray wavelength, half of the diffraction angle and full width at half maxima (FWHM) of the most intense peak, respectively. Small angle X-ray scattering studies were carried out on CBNP and GNP using Rigaku Ultima IV instrument in the transmission geometry (2θ range = $0\text{-}2.2^0$, step size = 0.01^0). The scattering intensity (I(q)) was measured as a function of scattering vector (q), where $q = 4\pi\sin\theta/\lambda$. The data analysis was performed using NANO-solver software and the parasitic scattering from air and sample cell was removed before data analysis. The hydrodynamic sizes of the dispersed nano-inclusions were measured from dynamic light scattering (DLS) studies. DLS

experiments were performed in the back-scattering geometry (178^0) using Zeta Nanosizer (Malvern Instrument). To probe the possible chemical reactions between the PCM and various nano-inclusions Fourier transform infrared (FTIR) spectroscopy was carried out in the wavenumber range of 900-3600 cm^{-1} using ABB Bomem MB 3000 FTIR spectrometer under attenuated total reflection (ATR) mode using ZnSe crystal. The solidification and melting temperatures and latent heat of fusion of the PCM were determined from differential scanning calorimetry (DSC) studies using Q200 (TA Instruments) in the temperature range of 0.1-80 ^{0}C with heating and cooling rates of 3 ^{0}C/minute under nitrogen atmosphere. Variations of refractive index of the PCM, as a function of temperature, was measured using an automatic refractometer (J357 series, Rudolph Research Analytical, USA). The automatic refractometer employs a LED light source of 589.3 nm wavelength and operates on the principle of critical angle measurement. The refractometer is capable of measuring refractive index from 1.26 to 1.70, as a function of temperature in the range of 15-100 ^{0}C, with measurement accuracies of 0.05 ^{0}C and 0.00004 for sample temperature and refractive index, respectively.

Section S6

Standardization of the transient hot wire method

Before proceeding with quantitative measurements, the KD2 probe was calibrated for three standard liquids, viz. water, kerosene and ethylene glycol. Using the KD2, at 27 ^{0}C, thermal conductivity of water, kerosene and ethylene glycol were estimated ~ 0.612 ± 0.005, 0.141 ± 0.003 and 0.261 ± 0.006 $Wm^{-1}K^{-1}$, which were found to be in good agreement with the standard thermal conductivity values of ~ 0.609, 0.145 and 0.258 $Wm^{-1}K^{-1}$ for water, kerosene and ethylene glycol, respectively. For performing the transient hot wire based thermal conductivity measurements, caution was exercised to follow the experimental protocols described in ASTM standard D7896-14 (Standard test method for thermal conductivity, thermal diffusivity and volumetric heat capacity of engine coolants and related fluids by transient hot wire liquid thermal conductivity method). Moreover, all the conditions highlight in ASTM standard D7896-14 were met, viz. a) thermal conductivity within the range of 0.1 to 1.0 Wm-1K-1, (b) no chemical reactions between platinum and fluid, (c) temperature range within the specified range of -20 to 100 ^{0}C and (d) no external pressurization. Additionally, thermal conductivity measurements were also carried out using hot disk thermal constant analyser (Model: TPS 2500s, Sweden) and results obtained from hot disk method and transient hot wire methods were found to be in very good agreement (maximum deviation was ~ ± 1.3 %). The above mentioned validation protocol was followed before proceeding with the quantitative measurements involving the phase change materials (with or without nano-inclusions).

Section S7

Description of the infrared camera used in the present study

In the present study, FLIR SC5000 infrared camera was used for non-contact temperature measurement, which is equipped with a 27 mm germanium made infrared transparent lens with field of view of $20^0 \times 16^0$ and indium antimonide (InSb) based (spectral range = 2.0-5.1 μm) focal plane array detector with 320 × 256 elements (Stirling cycle cooled).

Tables

Table S1
Absorption bands indicated in the FTIR spectra

Legend	Wave number (cm^{-1})	Description	Reference
(a)	2923	Asymmetric stretching of $–CH_2$ group	[30]
(b)	2855	Symmetric stretching of $–CH_2$ group	[30]
(c)	2362	Stretching vibration of C=O bond from atmospheric CO_2 interference	[30]
(d)	1716	Stretching of carbonyl group of free oleic acid	[30]
(e)	1667	Asymmetric stretching of $–COO^-$ group	[31]
(f)	1598	Symmetric stretching of $–COO^-$ group	[31]
(g)	1471	Asymmetric $–CH_3$ bend	[32]
(h)	1378	Symmetric $–CH_3$ bend	[32]

Table S2

Refractive index of hexadecane during solidification and melting

Process	Temperature (^{0}C)	Refractive Index	
		Value	Error
Solidification	25	1.43278	0.00004
	24	1.43319	0.00004
	22	1.43400	0.00004
	20	1.43482	0.00004
	19	1.43523	0.00004
	18	1.43564	0.00004
	17	1.43605	0.00004
	16	1.4354	0.0002
Melting	16	1.4354	0.0002
	17	1.43607	0.00007
	18	1.43566	0.00004
	19	1.43525	0.00004
	20	1.43486	0.00004
	22	1.43406	0.00004
	24	1.43326	0.00004
	25	1.43286	0.00004

Table S3

Thermal conductivity and enhancement in thermal conductivity of hexadecane as a function of temperature. Here, u(k) and u(k/k_f) indicate errors in thermal conductivity and k/k_f, respectively.

Temperature (^{0}C)	Thermal conductivity (k) ($Wm^{-1}K^{-1}$)	u(k) ($Wm^{-1}K^{-1}$)	k/k_f	u(k/k_f)
25	0.140	0.002	1.0000	0.0202
22	0.141	0.003	1.0071	0.0238
18.3	0.157	0.002	1.1214	0.0202
17.6	0.49	0.01	3.5000	0.1074
16	0.40	0.01	2.8429	0.0948
14.5	0.297	0.007	2.1214	0.0585
13.5	0.275	0.007	1.9643	0.0573
12	0.262	0.003	1.8714	0.0364
10	0.249	0.003	1.7786	0.0317
7	0.249	0.001	1.7786	0.0264
5	0.249	0.003	1.7786	0.0317

Table S4

Variation of thermal conductivity (k) and k/k_f as a function of temperature for different concentrations of CBNP loading in hexadecane. The units of thermal conductivity (k) and its standard uncertainty, u(k), are $Wm^{-1}K^{-1}$. k/k_f and its standard uncertainty, $u(k/k_f)$, are dimensionless.

Temperature (^{0}C)	PCM		0.001 wt. %		0.0025 wt. %		0.005 wt. %		0.0075 wt. %		0.01 wt. %	
	k	u(k)	k	u(k)	k	u(k)	k	u(k)	k	u(k)	k	u(k)
25	0.140	0.002	0.142	0.001	0.147	0.001	0.148	0.003	0.148	0.003	0.149	0.002
22	0.141	0.003	0.142	0.001	0.147	0.003	0.152	0.004	0.148	0.002	0.149	0.001
18.3	0.157	0.002	0.167	0.002	0.170	0.002	0.175	0.002	0.170	0.002	0.172	0.002
17.6	0.49	0.01	0.50	0.01	0.51	0.01	0.62	0.01	0.55	0.01	0.56	0.01
16	0.40	0.01	0.41	0.01	0.42	0.01	0.44	0.01	0.42	0.01	0.43	0.01
14.5	0.297	0.007	0.31	0.01	0.32	0.01	0.36	0.01	0.35	0.01	0.35	0.01
13.5	0.275	0.007	0.291	0.002	0.310	0.002	0.331	0.005	0.325	0.006	0.332	0.002
12	0.262	0.003	0.274	0.002	0.301	0.005	0.326	0.002	0.314	0.002	0.318	0.002
10	0.249	0.003	0.263	0.002	0.287	0.003	0.304	0.002	0.302	0.002	0.310	0.002
7	0.249	0.001	0.258	0.002	0.287	0.003	0.307	0.002	0.301	0.002	0.310	0.001
5	0.249	0.003	0.258	0.001	0.287	0.002	0.306	0.002	0.301	0.003	0.311	0.003
	k/k_f	$u(k/k_f)$	k/k_f	$u(k/k_f)$	k/k_f	$u(k/k_f)$	k/k_f	$u(k/k_f)$	k/k_f	$u(k/k_f)$	k/k_f	$u(k/k_f)$
25	1.0000	0.0202	1.0143	0.0162	1.0500	0.0166	1.0548	0.0235	1.0548	0.0235	1.0643	0.0196
22	1.0071	0.0238	1.0143	0.0162	1.0500	0.0241	1.0833	0.0312	1.0548	0.0186	1.0643	0.0168
18.3	1.1214	0.0202	1.1929	0.0211	1.2143	0.0213	1.2500	0.0217	1.2143	0.0225	1.2286	0.0215
17.6	3.5000	0.1074	3.6000	0.1062	3.6714	0.1129	4.3929	0.1223	3.9286	0.1103	4.0000	0.1139
16	2.8429	0.0948	2.9286	0.0922	3.0000	0.0958	3.1714	0.1033	3.0000	0.0990	3.0571	0.0994
14.5	2.1214	0.0585	2.2143	0.0717	2.2786	0.0714	2.5500	0.0751	2.5000	0.0748	2.5214	0.0756
13.5	1.9643	0.0573	2.0786	0.0322	2.2143	0.0347	2.3643	0.0507	2.3214	0.0556	2.3691	0.0356
12	1.8714	0.0364	1.9571	0.0306	2.1500	0.0487	2.3262	0.0371	2.2429	0.0344	2.2714	0.0355
10	1.7786	0.0317	1.8786	0.0304	2.0500	0.0349	2.1738	0.0352	2.1548	0.0342	2.2143	0.0347
7	1.7786	0.0264	1.8429	0.0291	2.0500	0.0349	2.1929	0.0337	2.1500	0.0339	2.2143	0.0324
5	1.7786	0.0317	1.8429	0.0273	2.0500	0.0349	2.1833	0.0353	2.1500	0.0361	2.2214	0.0369

Table S5

Variation of thermal conductivity (k) and k/k_f as a function of temperature for different concentrations of NiNP loading in hexadecane. The units of thermal conductivity (k) and its standard uncertainty, u(k), are $Wm^{-1}K^{-1}$. k/k_f and its standard uncertainty, $u(k/k_f)$, are dimensionless.

Temperature (^{0}C)	PCM		0.001 wt. %		0.0025 wt. %		0.005 wt. %		0.0075 wt. %		0.01 wt. %	
	k	u(k)	k	u(k)	k	u(k)	k	u(k)	k	u(k)	k	u(k)
25	0.140	0.002	0.143	0.001	0.146	0.001	0.148	0.002	0.147	0.001	0.143	0.003
22	0.141	0.003	0.144	0.001	0.151	0.001	0.150	0.002	0.148	0.001	0.144	0.002
18.3	0.157	0.002	0.165	0.002	0.169	0.001	0.170	0.002	0.167	0.006	0.169	0.002
17.6	0.49	0.01	0.49	0.01	0.52	0.01	0.58	0.01	0.58	0.01	0.57	0.01
16	0.40	0.01	0.43	0.01	0.48	0.01	0.50	0.01	0.50	0.01	0.52	0.01
14.5	0.297	0.007	0.33	0.01	0.35	0.01	0.37	0.01	0.34	0.01	0.35	0.01
13.5	0.275	0.007	0.300	0.001	0.325	0.002	0.345	0.002	0.321	0.002	0.330	0.003
12	0.262	0.003	0.280	0.002	0.301	0.002	0.322	0.003	0.298	0.002	0.310	0.002
10	0.249	0.003	0.260	0.002	0.283	0.002	0.298	0.002	0.282	0.002	0.284	0.003
7	0.249	0.001	0.258	0.002	0.283	0.002	0.297	0.002	0.282	0.002	0.284	0.001
5	0.249	0.003	0.258	0.001	0.283	0.003	0.297	0.001	0.282	0.001	0.284	0.002
	k/k_f	$u(k/k_f)$	k/k_f	$u(k/k_f)$	k/k_f	$u(k/k_f)$	k/k_f	$u(k/k_f)$	k/k_f	$u(k/k_f)$	k/k_f	$u(k/k_f)$
25	1.0000	0.0202	1.0214	0.0163	1.0429	0.0165	1.0571	0.0208	1.0500	0.0166	1.0214	0.0239
22	1.0071	0.0238	1.0286	0.0163	1.0786	0.0169	1.0714	0.0197	1.0571	0.0167	1.0286	0.0205
18.3	1.1214	0.0202	1.1786	0.0221	1.2071	0.0187	1.2143	0.0225	1.1929	0.0467	1.2048	0.0238
17.6	3.5000	0.1074	3.4786	0.1053	3.7286	0.1095	4.1286	0.1112	4.1643	0.1091	4.1000	0.1104
16	2.8429	0.0948	3.0714	0.0982	3.4143	0.1017	3.5786	0.1017	3.5786	0.0925	3.7143	0.1057
14.5	2.1214	0.0585	2.3214	0.0781	2.5000	0.0824	2.6429	0.0802	2.4571	0.0611	2.5214	0.0781
13.5	1.9643	0.0573	2.1429	0.0314	2.3214	0.0361	2.4643	0.0373	2.2929	0.0350	2.3571	0.0386
12	1.8714	0.0364	2.0000	0.0319	2.1500	0.0331	2.3000	0.0379	2.1286	0.0336	2.2143	0.0347
10	1.7786	0.0317	1.8571	0.0293	2.0214	0.0314	2.1286	0.0328	2.0143	0.0321	2.0286	0.0346
7	1.7786	0.0264	1.8429	0.0291	2.0214	0.0322	2.1214	0.0335	2.0143	0.0321	2.0286	0.0299
5	1.7786	0.0317	1.8429	0.0273	2.0214	0.0345	2.1214	0.0311	2.0143	0.0297	2.0286	0.0323

Table S6

Variation of thermal conductivity (k) and k/k_f as a function of temperature for different concentrations of CuNP loading in hexadecane. The units of thermal conductivity (k) and its standard uncertainty, u(k), are $Wm^{-1}K^{-1}$. k/k_f and its standard uncertainty, $u(k/k_f)$, are dimensionless.

Temperature (^{0}C)	PCM		0.001 wt. %		0.0025 wt. %		0.005 wt. %		0.0075 wt. %		0.01 wt. %	
	k	u(k)	k	u(k)	k	u(k)	k	u(k)	k	u(k)	k	u(k)
25	0.140	0.002	0.144	0.002	0.148	0.003	0.153	0.001	0.154	0.001	0.156	0.001
22	0.141	0.003	0.146	0.001	0.149	0.001	0.154	0.001	0.156	0.003	0.157	0.002
18.3	0.157	0.002	0.160	0.002	0.169	0.001	0.171	0.003	0.173	0.001	0.173	0.002
17.6	0.49	0.01	0.56	0.01	0.46	0.01	0.45	0.01	0.54	0.01	0.63	0.01
16	0.40	0.01	0.43	0.01	0.42	0.01	0.40	0.01	0.44	0.01	0.47	0.01
14.5	0.297	0.007	0.34	0.01	0.34	0.01	0.34	0.01	0.34	0.01	0.35	0.01
13.5	0.275	0.007	0.305	0.002	0.310	0.002	0.326	0.004	0.319	0.001	0.345	0.004
12	0.262	0.003	0.280	0.002	0.277	0.001	0.291	0.001	0.297	0.002	0.321	0.003
10	0.249	0.003	0.260	0.002	0.263	0.002	0.281	0.002	0.284	0.003	0.304	0.003
7	0.249	0.001	0.260	0.003	0.263	0.002	0.277	0.001	0.284	0.001	0.302	0.002
5	0.249	0.003	0.259	0.001	0.262	0.003	0.277	0.003	0.283	0.001	0.302	0.001
	k/k_f	$u(k/k_f)$	k/k_f	$u(k/k_f)$	k/k_f	$u(k/k_f)$	k/k_f	$u(k/k_f)$	k/k_f	$u(k/k_f)$	k/k_f	$u(k/k_f)$
25	1.0000	0.0202	1.0286	0.0192	1.0571	0.0242	1.0929	0.0172	1.1000	0.0173	1.1143	0.0175
22	1.0071	0.0238	1.0429	0.0165	1.0643	0.0168	1.1000	0.0173	1.1143	0.0247	1.1214	0.0202
18.3	1.1214	0.0202	1.1429	0.0205	1.2071	0.0187	1.2214	0.0257	1.2357	0.0190	1.2357	0.0216
17.6	3.5000	0.1074	4.0071	0.1103	3.3143	0.1152	3.2143	0.1133	3.8286	0.1047	4.4786	0.1128
16	2.8429	0.0948	3.0714	0.0931	3.0143	0.1024	2.8286	0.0993	3.1143	0.0940	3.3214	0.0974
14.5	2.1214	0.0585	2.4143	0.0749	2.4500	0.0738	2.4500	0.0783	2.4429	0.0782	2.5214	0.0768
13.5	1.9643	0.0573	2.1786	0.0335	2.2143	0.0339	2.3286	0.0421	2.2786	0.0333	2.4643	0.0436
12	1.8714	0.0364	2.0000	0.0319	1.9786	0.0292	2.0786	0.0305	2.1214	0.0327	2.2929	0.0411
10	1.7786	0.0317	1.8548	0.0287	1.8786	0.0296	2.007	0.0312	2.0286	0.0346	2.1714	0.0363
7	1.7786	0.0264	1.8595	0.0321	1.8786	0.0296	1.9786	0.0292	2.0286	0.0299	2.1571	0.0339
5	1.7786	0.0317	1.8476	0.0277	1.8714	0.0327	1.9786	0.0340	2.0214	0.0298	2.1571	0.0316

Table S7

Variation of thermal conductivity (k) and k/k_f as a function of temperature for different concentrations of AgNW loading in hexadecane. The units of thermal conductivity (k) and its standard uncertainty, u(k), are $Wm^{-1}K^{-1}$. k/k_f and its standard uncertainty, $u(k/k_f)$, are dimensionless.

Temperature (^{0}C)	PCM		0.001 wt. %		0.0025 wt. %		0.005 wt. %		0.0075 wt. %		0.01 wt. %	
	k	u(k)	k	u(k)	k	u(k)	k	u(k)	k	u(k)	k	u(k)
25	0.140	0.002	0.144	0.002	0.150	0.002	0.144	0.001	0.152	0.002	0.153	0.001
22	0.141	0.003	0.146	0.002	0.151	0.001	0.144	0.001	0.152	0.001	0.153	0.001
18.3	0.157	0.002	0.162	0.001	0.169	0.002	0.169	0.001	0.167	0.004	0.167	0.003
17.6	0.49	0.01	0.68	0.01	0.61	0.01	0.59	0.01	0.54	0.01	0.63	0.01
16	0.40	0.01	0.39	0.01	0.49	0.01	0.44	0.01	0.48	0.01	0.52	0.01
14.5	0.297	0.007	0.33	0.01	0.37	0.01	0.37	0.01	0.32	0.01	0.35	0.01
13.5	0.275	0.007	0.300	0.002	0.331	0.002	0.345	0.004	0.301	0.001	0.346	0.002
12	0.262	0.003	0.276	0.002	0.314	0.002	0.325	0.006	0.287	0.002	0.324	0.002
10	0.249	0.003	0.263	0.001	0.304	0.002	0.321	0.001	0.283	0.001	0.305	0.002
7	0.249	0.001	0.263	0.002	0.304	0.001	0.319	0.003	0.282	0.002	0.298	0.002
5	0.249	0.003	0.263	0.002	0.303	0.001	0.312	0.003	0.282	0.001	0.296	0.002
	k/k_f	$u(k/k_f)$	k/k_f	$u(k/k_f)$	k/k_f	$u(k/k_f)$	k/k_f	$u(k/k_f)$	k/k_f	$u(k/k_f)$	k/k_f	$u(k/k_f)$
25	1.0000	0.0202	1.0286	0.0192	1.0714	0.0197	1.0286	0.0163	1.0857	0.0198	1.0929	0.0172
22	1.0071	0.0238	1.0429	0.0194	1.0786	0.0169	1.0286	0.0163	1.0857	0.0171	1.0929	0.0172
18.3	1.1214	0.0202	1.1571	0.0180	1.2071	0.0212	1.2071	0.0187	1.1929	0.0309	1.1929	0.0255
17.6	3.5000	0.1074	4.8214	0.1244	4.3714	0.0119	4.2571	0.1134	3.8714	0.1174	4.4786	0.1145
16	2.8429	0.0948	2.7786	0.0997	3.5286	0.1025	3.1214	0.0935	3.4000	0.1054	3.7071	0.1002
14.5	2.1214	0.0585	2.3286	0.0775	2.6286	0.0871	2.6214	0.0788	2.2786	0.0733	2.5214	0.0768
13.5	1.9643	0.0573	2.1429	0.0338	2.3643	0.0367	2.4643	0.0436	2.1500	0.0315	2.4714	0.0381
12	1.8714	0.0364	1.9714	0.0308	2.2429	0.0344	2.3214	0.0556	2.0500	0.0318	2.3143	0.0360
10	1.7786	0.0317	1.8786	0.0268	2.1714	0.0334	2.2929	0.0335	2.0214	0.0298	2.1786	0.0342
7	1.7786	0.0264	1.8786	0.0304	2.1714	0.0318	2.2786	0.0376	2.0143	0.0313	2.1286	0.0336
5	1.7786	0.0317	1.8786	0.0296	2.1643	0.0317	2.2286	0.0370	2.0143	0.0297	2.1143	0.0326

Table S8

Variation of thermal conductivity (k) and k/k_f as a function of temperature for different concentrations of MWCNT loading in hexadecane. The units of thermal conductivity (k) and its standard uncertainty, u(k), are $Wm^{-1}K^{-1}$. k/k_f and its standard uncertainty, $u(k/k_f)$, are dimensionless.

Temperature (^{0}C)	PCM		0.001 wt. %		0.0025 wt. %		0.005 wt. %		0.0075 wt. %		0.01 wt. %	
	k	u(k)	k	u(k)	k	u(k)	k	u(k)	k	u(k)	k	u(k)
25	0.140	0.002	0.142	0.001	0.144	0.001	0.146	0.001	0.147	0.001	0.148	0.002
22	0.141	0.003	0.143	0.001	0.144	0.002	0.147	0.002	0.148	0.001	0.149	0.001
18.3	0.157	0.002	0.160	0.002	0.169	0.001	0.176	0.002	0.169	0.004	0.174	0.002
17.6	0.49	0.01	0.47	0.01	0.51	0.01	0.52	0.01	0.52	0.01	0.43	0.01
16	0.40	0.01	0.43	0.01	0.47	0.01	0.43	0.01	0.47	0.01	0.37	0.01
14.5	0.297	0.007	0.36	0.01	0.34	0.01	0.34	0.01	0.38	0.01	0.35	0.01
13.5	0.275	0.007	0.310	0.002	0.316	0.002	0.315	0.003	0.351	0.003	0.291	0.002
12	0.262	0.003	0.262	0.003	0.277	0.003	0.280	0.002	0.301	0.003	0.269	0.002
10	0.249	0.003	0.252	0.002	0.259	0.001	0.263	0.002	0.287	0.002	0.263	0.002
7	0.249	0.001	0.252	0.001	0.258	0.002	0.262	0.003	0.284	0.002	0.263	0.003
5	0.249	0.003	0.252	0.002	0.258	0.003	0.262	0.001	0.284	0.001	0.263	0.002
	k/k_f	**$u(k/k_f)$**	**k/k_f**	**$u(k/k_f)$**	**k/k_f**	**$u(k/k_f)$**	**k/k_f**	**$u(k/k_f)$**	**k/k_f**	**$u(k/k_f)$**	**k/k_f**	**$u(k/k_f)$**
25	1.0000	0.0202	1.0143	0.0162	1.0286	0.0163	1.0429	0.0165	1.0500	0.0166	1.0571	0.0195
22	1.0071	0.0238	1.0214	0.0163	1.0286	0.0205	1.0500	0.0207	1.0571	0.0167	1.0643	0.0168
18.3	1.1214	0.0202	1.1429	0.0217	1.2071	0.0187	1.2571	0.0229	1.2071	0.0309	1.2429	0.0228
17.6	3.5000	0.1074	3.3786	0.0928	3.6429	0.1003	3.7286	0.0891	3.7357	0.1134	3.0929	0.0996
16	2.8429	0.0948	3.0643	0.0868	3.3214	0.0918	3.0786	0.0963	3.3786	0.1047	2.6429	0.0891
14.5	2.1214	0.0585	2.6000	0.0779	2.4286	0.0756	2.4286	0.0775	2.6786	0.0874	2.5214	0.0787
13.5	1.9643	0.0573	2.2143	0.0347	2.2571	0.0345	2.2500	0.0373	2.5071	0.0405	2.0786	0.0322
12	1.8714	0.0364	1.8714	0.0327	1.9786	0.0340	2.0000	0.0319	2.1500	0.0361	1.9214	0.0301
10	1.7786	0.0317	1.8000	0.0294	1.8500	0.0274	1.8786	0.0296	2.0500	0.0326	1.8786	0.0304
7	1.7786	0.0264	1.8000	0.0267	1.8429	0.0299	1.8714	0.0327	2.0286	0.0323	1.8786	0.0328
5	1.7786	0.0317	1.8000	0.0294	1.8429	0.0324	1.8714	0.0277	2.0286	0.0299	1.8786	0.0304

Table S9

Variation of thermal conductivity (k) and k/k_f as a function of temperature for different concentrations of GNP loading in hexadecane. The units of thermal conductivity (k) and its standard uncertainty, u(k), are $Wm^{-1}K^{-1}$. k/k_f and its standard uncertainty, $u(k/k_f)$, are dimensionless.

Temperature (^{0}C)	PCM		0.001 wt. %		0.0025 wt. %		0.005 wt. %		0.0075 wt. %		0.01 wt. %	
	k	u(k)	k	u(k)	k	u(k)	k	u(k)	k	u(k)	k	u(k)
25	0.140	0.002	0.142	0.001	0.144	0.001	0.146	0.003	0.148	0.001	0.150	0.002
22	0.141	0.003	0.142	0.001	0.144	0.002	0.147	0.001	0.148	0.003	0.148	0.002
18.3	0.157	0.002	0.160	0.002	0.161	0.003	0.165	0.003	0.170	0.003	0.171	0.002
17.6	0.49	0.01	0.50	0.01	0.51	0.01	0.52	0.01	0.53	0.01	0.54	0.01
16	0.40	0.01	0.42	0.01	0.42	0.01	0.43	0.01	0.43	0.01	0.43	0.01
14.5	0.297	0.007	0.31	0.01	0.31	0.01	0.32	0.01	0.33	0.01	0.35	0.01
13.5	0.275	0.007	0.280	0.003	0.290	0.003	0.305	0.002	0.312	0.003	0.319	0.001
12	0.262	0.003	0.270	0.004	0.272	0.002	0.291	0.004	0.298	0.002	0.308	0.002
10	0.249	0.003	0.258	0.002	0.268	0.002	0.280	0.002	0.290	0.002	0.296	0.001
7	0.249	0.001	0.256	0.003	0.268	0.002	0.277	0.002	0.288	0.003	0.295	0.003
5	0.249	0.003	0.256	0.001	0.270	0.001	0.277	0.001	0.287	0.003	0.294	0.001
	k/k_f	$u(k/k_f)$	k/k_f	$u(k/k_f)$	k/k_f	$u(k/k_f)$	k/k_f	$u(k/k_f)$	k/k_f	$u(k/k_f)$	k/k_f	$u(k/k_f)$
25	1.0000	0.0202	1.0143	0.0162	1.0286	0.0163	1.0429	0.0241	1.0571	0.0167	1.0714	0.0197
22	1.0071	0.0238	1.0143	0.0145	1.0286	0.0192	1.0500	0.0150	1.0571	0.0242	1.0571	0.0195
18.3	1.1214	0.0202	1.1429	0.0217	1.1500	0.0250	1.1786	0.0253	1.2143	0.0257	1.2214	0.0214
17.6	3.5000	0.1074	3.5714	0.1078	3.6286	0.1064	3.7143	0.1082	3.7786	0.1099	3.8214	0.1077
16	2.8429	0.0948	2.9643	0.0963	3.0000	0.0946	3.0571	0.0962	3.0714	0.0995	3.0929	0.0983
14.5	2.1214	0.0585	2.2000	0.0761	2.2286	0.0743	2.2500	0.0738	2.3214	0.0729	2.5214	0.0768
13.5	1.9643	0.0573	2.0000	0.0357	2.0714	0.0351	2.1786	0.0342	2.2286	0.0370	2.2786	0.0333
12	1.8714	0.0364	1.9286	0.0377	1.9429	0.0304	2.0786	0.0393	2.1286	0.0336	2.2000	0.0338
10	1.7786	0.0317	1.8429	0.0299	1.9143	0.0309	2.0000	0.0311	2.0714	0.0329	2.1143	0.0310
7	1.7786	0.0264	1.8286	0.0338	1.9143	0.0309	1.9786	0.0309	2.0571	0.0349	2.1071	0.0369
5	1.7786	0.0317	1.8286	0.0271	1.9286	0.0285	1.9786	0.0292	2.0500	0.0349	2.1000	0.0308

Table S10

Variation of thermal conductivity (k) and k/k_f as a function of temperature for different concentrations of GNP-UC loading in hexadecane. The units of thermal conductivity (k) and its standard uncertainty, u(k), are $Wm^{-1}K^{-1}$. k/k_f and its standard uncertainty, $u(k/k_f)$, are dimensionless.

Temperature (^{0}C)	PCM		0.001 wt. %		0.0025 wt. %		0.005 wt. %		0.0075 wt. %		0.01 wt. %	
	k	u(k)	k	u(k)	k	u(k)	k	u(k)	k	u(k)	k	u(k)
25	0.140	0.002	0.140	0.002	0.144	0.001	0.146	0.001	0.151	0.001	0.148	0.002
22	0.141	0.003	0.142	0.001	0.144	0.001	0.146	0.001	0.153	0.002	0.148	0.001
18.3	0.157	0.002	0.165	0.002	0.167	0.003	0.168	0.002	0.165	0.002	0.165	0.001
17.6	0.49	0.01	0.56	0.01	0.54	0.01	0.53	0.01	0.53	0.01	0.56	0.01
16	0.40	0.01	0.41	0.01	0.45	0.01	0.45	0.01	0.48	0.01	0.45	0.01
14.5	0.297	0.007	0.31	0.01	0.36	0.01	0.37	0.01	0.37	0.01	0.35	0.01
13.5	0.275	0.007	0.290	0.003	0.331	0.003	0.342	0.004	0.345	0.003	0.305	0.003
12	0.262	0.003	0.263	0.002	0.304	0.002	0.312	0.003	0.319	0.002	0.279	0.003
10	0.249	0.003	0.256	0.003	0.288	0.002	0.288	0.002	0.310	0.002	0.265	0.003
7	0.249	0.001	0.256	0.002	0.284	0.001	0.288	0.001	0.308	0.002	0.265	0.001
5	0.249	0.003	0.256	0.001	0.282	0.001	0.288	0.004	0.308	0.001	0.262	0.002
	k/k_f	$u(k/k_f)$	k/k_f	$u(k/k_f)$	k/k_f	$u(k/k_f)$	k/k_f	$u(k/k_f)$	k/k_f	$u(k/k_f)$	k/k_f	$u(k/k_f)$
25	1.0000	0.0202	1.0000	0.0189	1.0286	0.0163	1.0429	0.0165	1.0786	0.0169	1.0571	0.0195
22	1.0071	0.0238	1.0143	0.0162	1.0286	0.0163	1.0429	0.0165	1.0929	0.0199	1.0571	0.0167
18.3	1.1214	0.0202	1.1786	0.0221	1.1929	0.0255	1.2000	0.0223	1.1786	0.0221	1.1786	0.0183
17.6	3.5000	0.1074	4.0000	0.1121	3.8286	0.1029	3.7929	0.1119	3.8000	0.1138	3.9929	0.1151
16	2.8429	0.0948	4.8929	0.0875	3.2000	0.0928	3.1929	0.0939	3.4143	0.0992	3.2071	0.0972
14.5	2.1214	0.0585	2.2143	0.0736	2.5714	0.0740	2.6500	0.0739	2.6071	0.0806	2.5214	0.0832
13.5	1.9643	0.0573	2.0714	0.0351	2.3643	0.0387	2.4429	0.0434	2.4643	0.0399	2.1786	0.0364
12	1.8714	0.0364	1.8786	0.0304	2.1714	0.0342	2.2286	0.0370	2.2786	0.0348	1.9929	0.0342
10	1.7786	0.0317	1.8286	0.0322	2.0571	0.0327	2.0571	0.0319	2.2143	0.0347	1.8929	0.0345
7	1.7786	0.0264	1.8286	0.0298	2.0286	0.0299	2.0571	0.0302	2.2000	0.0338	1.8929	0.0279
5	1.7786	0.0317	1.8286	0.0271	2.0143	0.0297	2.0571	0.0391	2.2000	0.0322	1.8714	0.0295

Figures

Figure S1

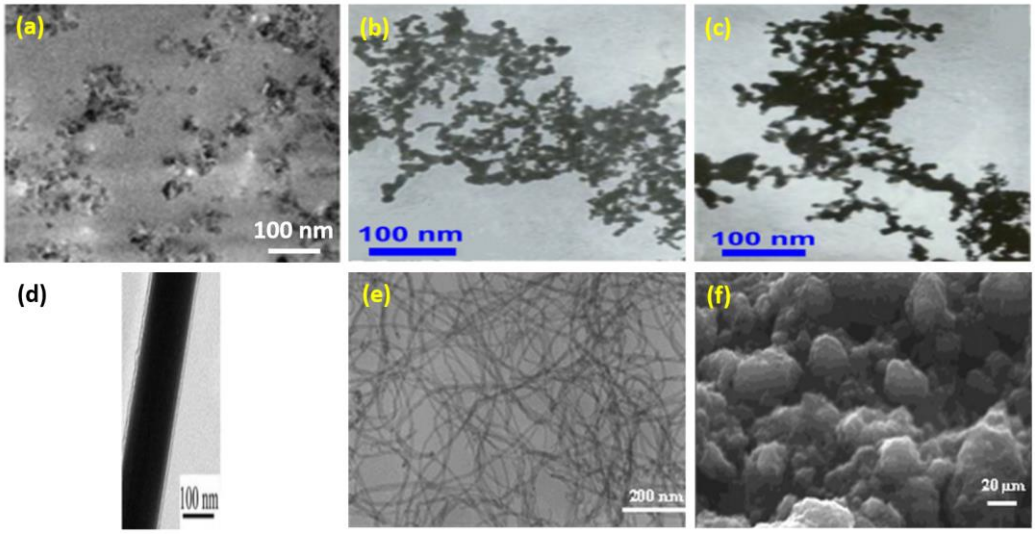

Figure S1 TEM images of (a) CBNP, (b) NiNP, (c) CuNP, (d) AgNW and (e) MWCNT nano-inclusions. (f) SEM image of GNP nano-inclusion. The scale bars are shown along with the electron microscopy images, which were obtained from the respective suppliers.

Figure S2

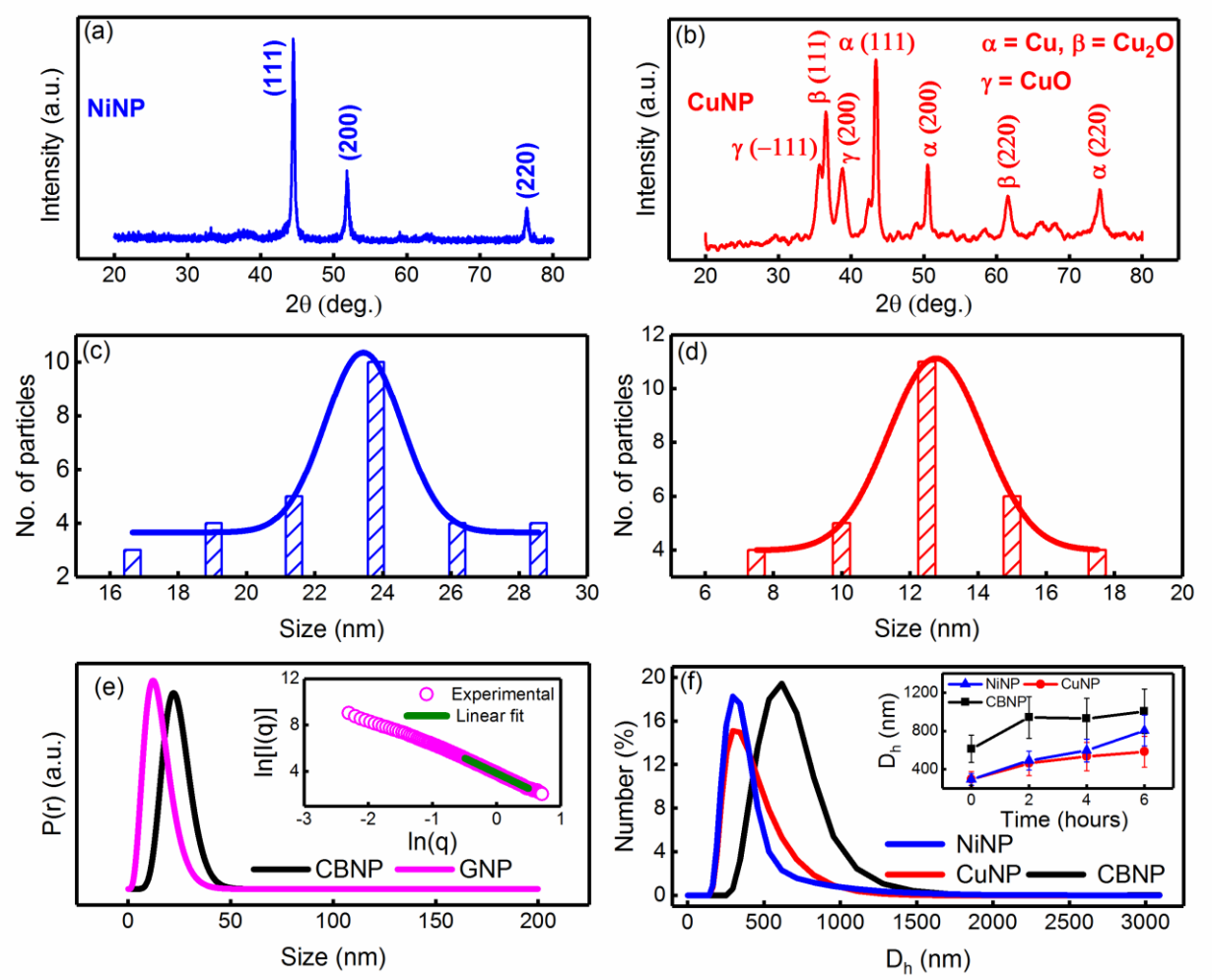

Figure S2 Room temperature powder XRD pattern of (a) NiNP and (b) CuNP nano-inclusions, where the Bragg reflection peak are indexed. The average crystallite sizes, determined from the strongest reflection peak of (111) using Scherrer's equation, were ~ 29 (±3) and 13 (±2) nm for NiNP and CuNP, respectively. Size distributions for the (c) NiNP and (d) CuNP nano-inclusions obtained from TEM image analyses (Figs. 1b-c, respectively). The average sizes were obtained as 23.4 ± 2.3 and 12.8 ± 2.8 nm for NiNP and CuNP, respectively. (e) Distance distribution function [P(r)], obtained from SAXS, as a function of size for CBNP and GNP nano-inclusions. The most probable sizes were found to be 21 (± 2) and 12.3 (± 2) nm, respectively. (Inset) Variation of ln[I(q)] as a function of ln(q) in the case of GNP and the linear regression analysis of the experimental data for the high q region (Porod's region). The slope and adjusted R^2 of the linear regression analysis were ~ -2.63 (±0.001) and 0.99, respectively. (f) Hydrodynamic size distributions of NiNP, CuNP and CBNP nano-inclusions, dispersed in hexadecane at room temperature. The average hydrodynamic sizes were ~ 295 ± 59, 296 ± 82 and 615 ± 141 nm, respectively. (Inset) The variation of average hydrodynamic sizes of NiNP, CuNP and CBNP nano-inclusions as a function of time.

Figure S3

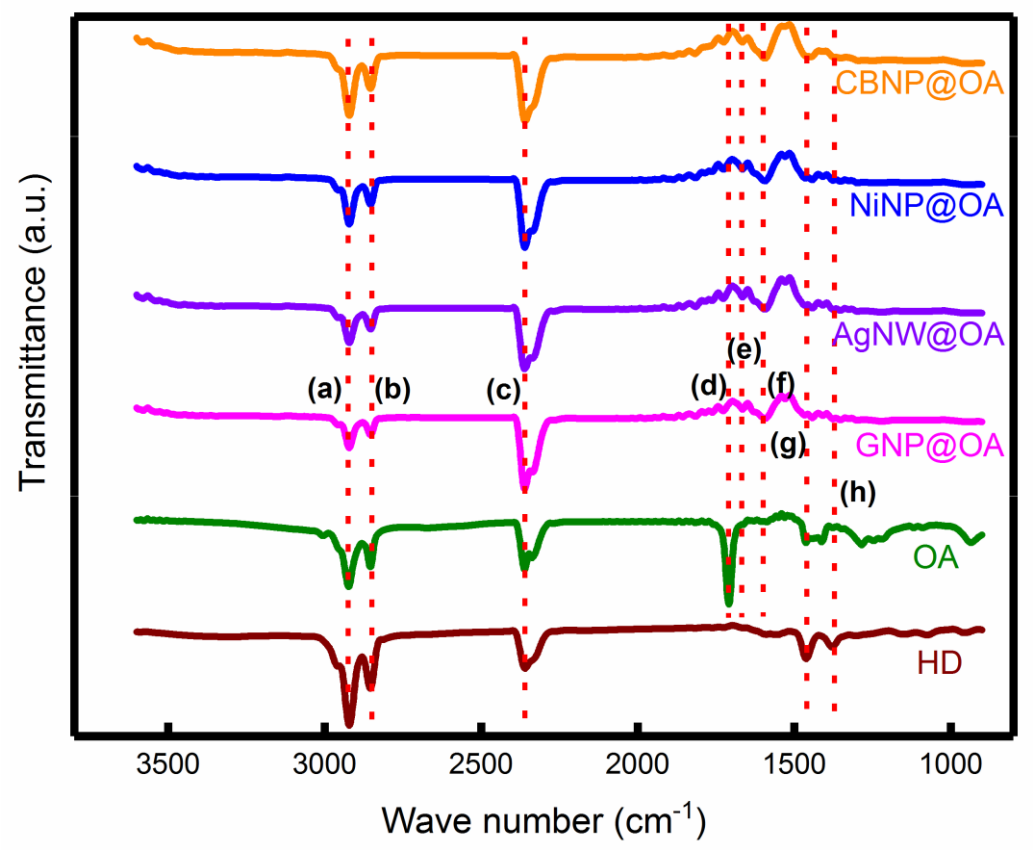

Figure S3 FTIR spectra of the oleic acid capped CBNP, NiNP, AgNW, and GNP nano-inclusions, dispersed in hexadecane. For comparison, the FTIR spectra of pure oleic acid (OA) and hexadecane (HD) are also shown in the figure. The major absorption bands are indexed and Table 1 shows the details.

Figure S4

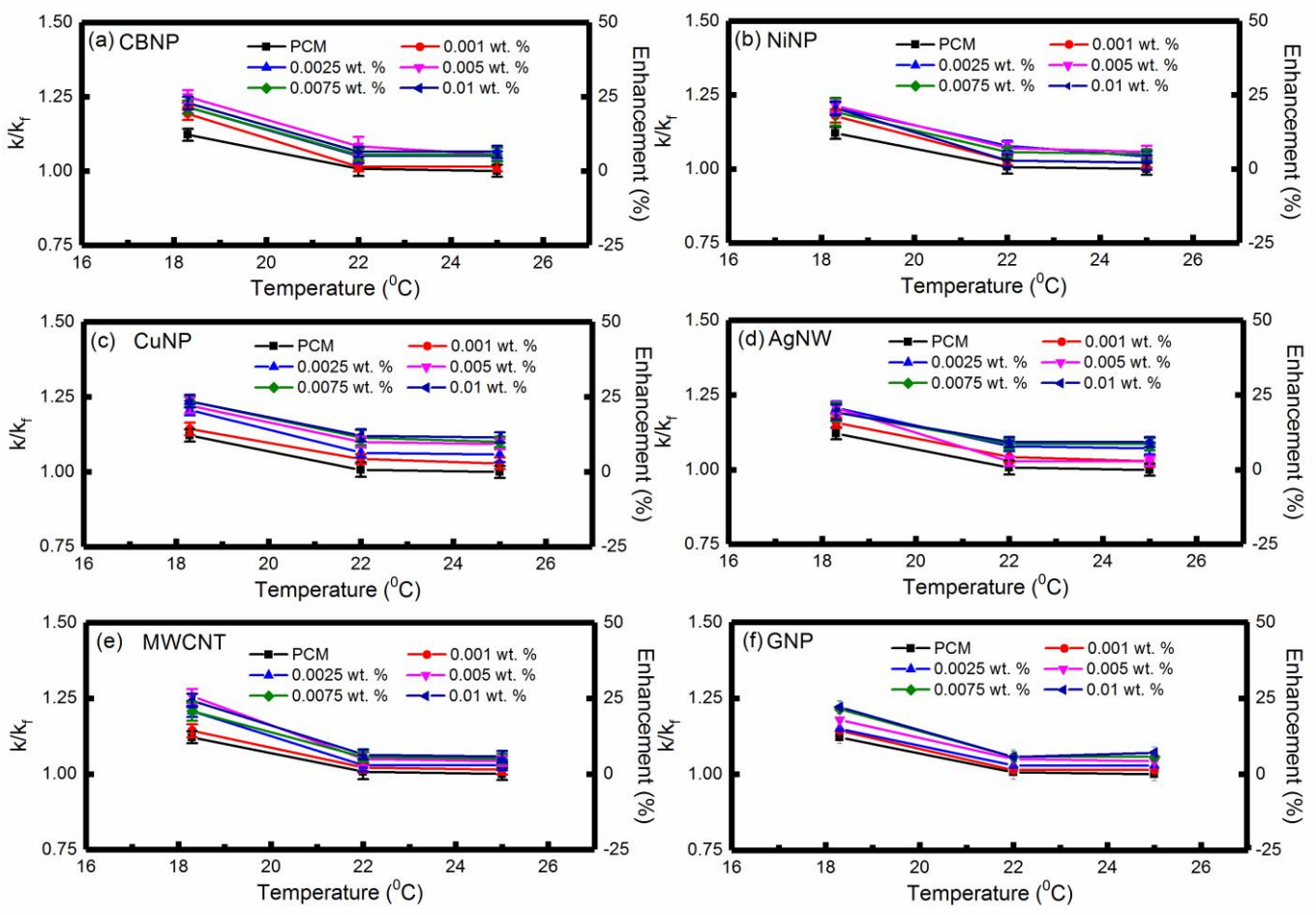

Figure S4 Enlarged view of the variation of k/k_f and percentage enhancement of liquid state thermal conductivity, as a function of temperature, for the PCM loaded with various concentrations of (a) CBNP, (b) NiNP, (c) CuNP, (d) AgNW, (e) MWCNT and (f) GNP.

Figure S5

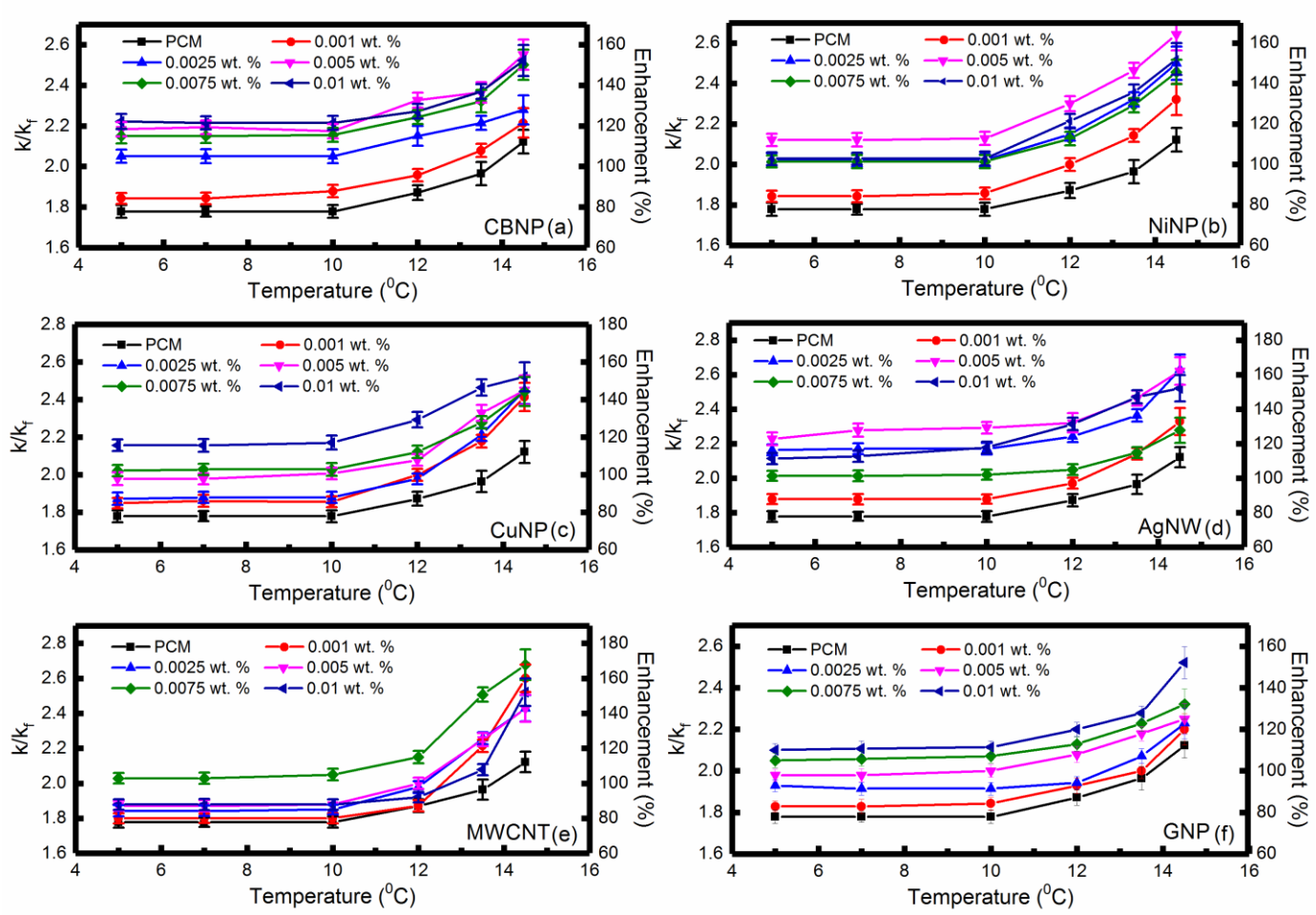

Figure S5 Enlarged view of the variation of k/k_f and percentage enhancement of solid state thermal conductivity, as a function of temperature, for the PCM loaded with various concentrations of (a) CBNP, (b) NiNP, (c) CuNP, (d) AgNW, (e) MWCNT and (f) GNP.

Figure S6

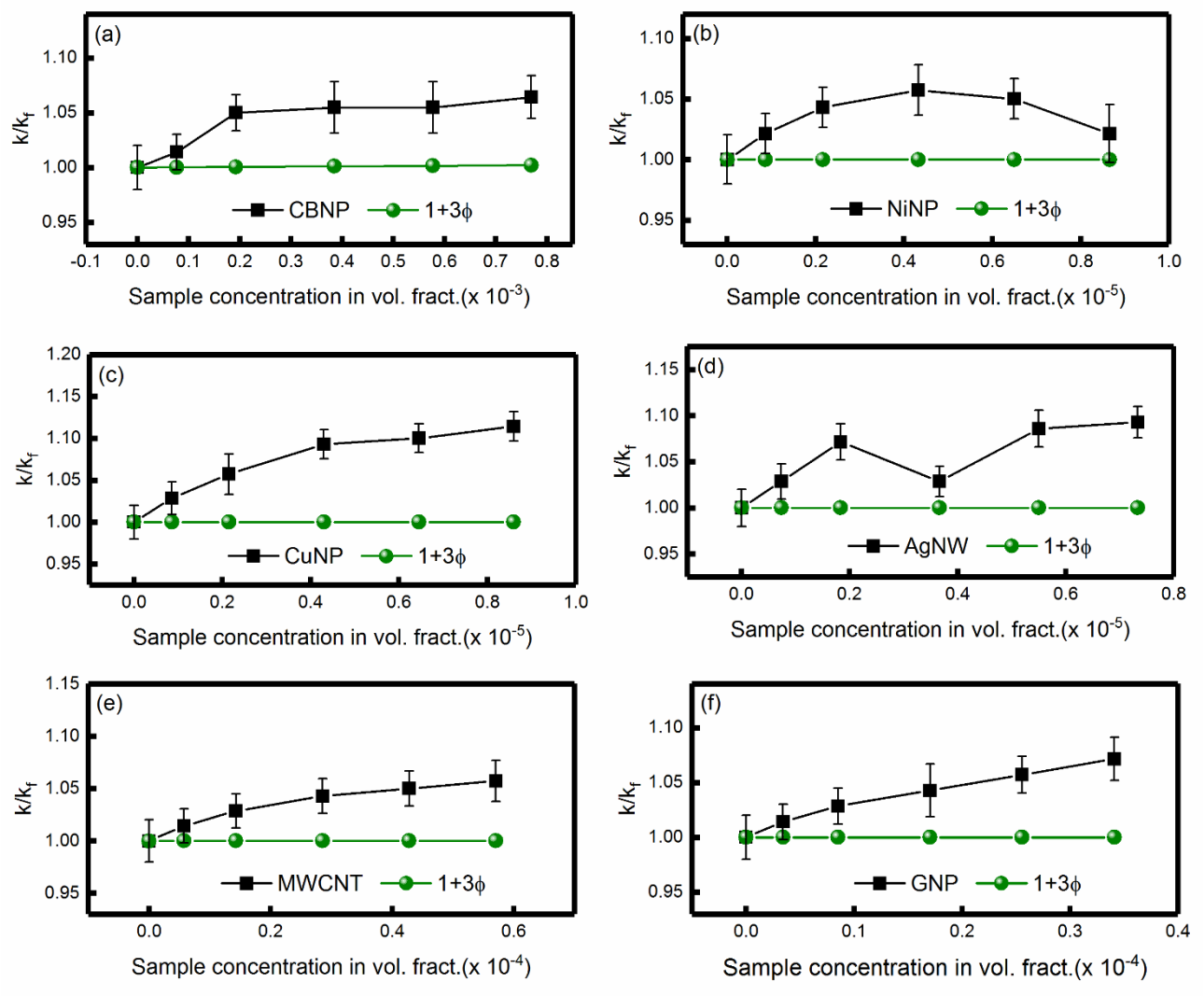

Figure S6 Variation of k/k_f, in the liquid state, as a function of concentration (in volume fraction), for the PCM loaded with (a) CBNP, (b) NiNP, (c) CuNP, (d) AgNW, (e) MWCNT and (f) GNP nano-inclusions. The theoretical plots, for the effective medium theory ($k/k_f = 1+3\phi$, ϕ being volume fraction of the nano-inclusions) are also shown.

Figure S7

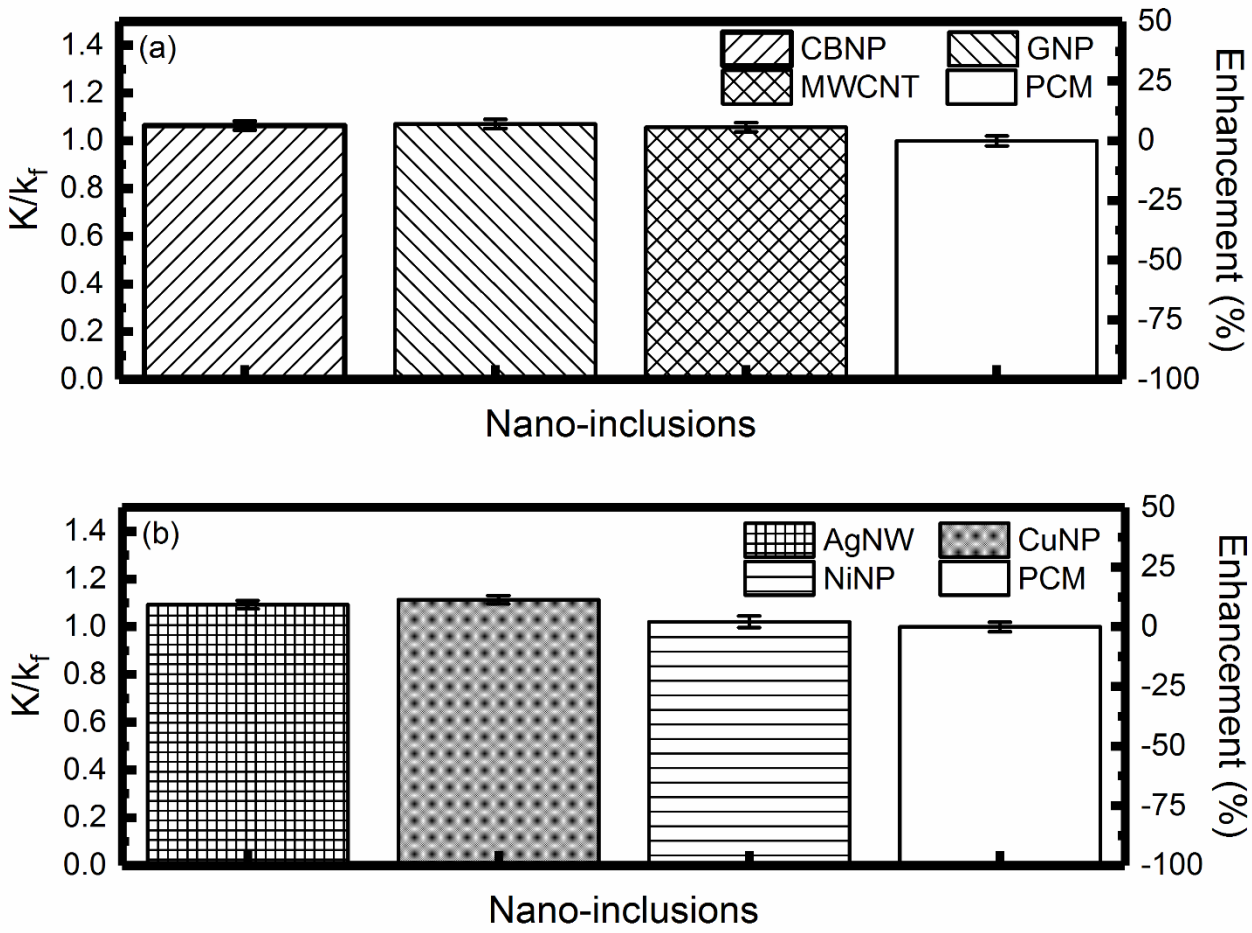

Figure S7 Bar charts comparing the thermal conductivity enhancements in the liquid state for the PCM loaded with (a) carbon-based and (b) metallic nano-inclusions. For comparison, the thermal conductivity enhancement of the PCM, without any nano-inclusions, is shown in both figures.

Figure S8

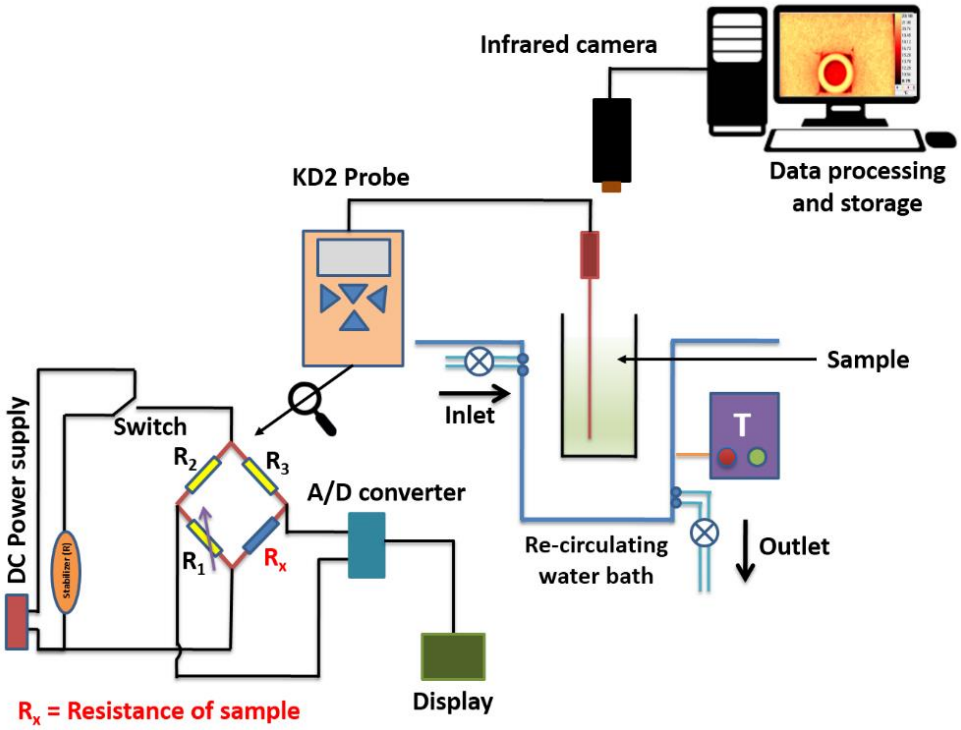

Figure S8 Typical schematic of the experimental set-up. The infrared camera, transient hot wire probe (KD2 probe), recirculating water bath, sample location and data acquisition systems are indicated in the schematic.